Journal of Applied Polymer Science

A Comparative Study on Effect of Aromatic Polyimide Chain Conformation on Reinforcement of Carbon Nanotube/Polyimide Nanocomposites

Baode Zhang,[1] Ali Nabipour Chakoli,[2,3] Wanchen Zang,[4] Yanqing Tian,[5] Ke Zhang,[2] Chunhai Chen,[4] Yao Li[1]

[1]Center for Composite Materials, Harbin Institute of Technology, Harbin 150008, China
[2]School of Chemical Engineering and Technology, Harbin Institute of Technology, Harbin 150001, China
[3]Agricultural, Medical and Industrial Research School, NSTRI, Karaj, Iran
[4]Alan G. MacDiarmid Institute, Jilin University, Chang Chun 130012, China
[5]Biodesign Institute, Arizona State University, Tempe, Arizona 85287
Correspondence to: B. Zhang (E-mail: zhangbaode@hit.edu.cn) and Y. Li (E-mail: yaoli@hit.edu.cn)

ABSTRACT: Two kinds of polyimides (PIs) were selected as matrices for multiwalled carbon nanotubes (CNTs)-based nanocomposites. The two PIs were initially synthesized through reactions of a same benzoxazole-containing diamine with two different dianhydrids. A linear PI was formed from the ether bond-containing dianhydride, while a nonlinear PI was formed from the —$C(CF3)_2$– groups containing dianhydride. Optimized dispersion of nanotubes in both kinds of PIs was found to be at a concentration with 0.5 wt % COOH-CNT, where great enhancement was achieved for both PIs. It was also found that introducing nanotubes into PI matrices aroused more significant increase of Young's modulus and break stress in linear PI than that in nonlinear PI. To determine the key parameters involved in design of PIs for maximum reinforcement efficiency using CNT as the nanofiller, the nanoscopic dispersion state of the nanotubes in diamine solution and their reaction were investigated via morphological and spectroscopic studies. The interfacial interactions between nanotubes and two PI chains were characterized by FT-IR and Raman spectroscopy. The fracture surface characteristics of two series of CNT/PI nanocomposites were further investigated using SEM. Our findings show that the diamine plays a double role for the in-situ polymerization, a dispersant to disentangle the CNT agglomerates and a monomer for PI synthesis with dianhydrides. It was also found that geometry and flexibility of PI chains are crucial to determine the interfacial interactions between nanotubes and PI chains. For elucidating the different interfacial characteristics of the two PIs on the surface of CNT, we proposed a model for preferred conformation adopted by a single PI chain on a single CNT. © 2014 Wiley Periodicals, Inc. J. Appl. Polym. Sci. **2014**, *131*, 40479.

KEYWORDS: composites; nanotubes; graphene and fullerenes; morphology; polyimides

Received 18 November 2013; accepted 19 January 2014
DOI: 10.1002/app.40479

INTRODUCTION

Aromatic PI has served as martrix for composites due to an excellent combination of thermal stablility and mechanical property.[1–3] The superior properties of CNTs composing entirely sp^2 carbon—carbon bonds have sparked interests in the promising application of fier reinforced composite materials for improving mechanical, electric and thermal properties.[4,5] The combination of CNTs and PIs is expected to create novel multifunctional nanocomposites.[6–8] However, the performance of CNT/PI nanocomposites depends on the dispersion of CNTs in the PI matrix and interfacial interactions between CNTs and the PIs. The CNTs are generally insoluble because of their rather weak interactions with common polymers and severely tangle with each other due to electrostatic and van der Waals force among them. The formation of bundled and agglomerated structures results in diminished mechanical and electrical properties. Significant research efforts have been directed toward the proper dispersion of CNT in PI and the appropriate interfacial interactions between nanotubes and PI chains.[9–11] Surface modification, covalent bonding of functional group and noncovalent wrapping or adsorption of mediating molecules on to the CNT surface have been explored to improve the dispersibility of CNTs.[12–14] Cheo et al. achieved an efficient dispersion of single-walled CNT bundles in a PI matrix through the π–π overlap

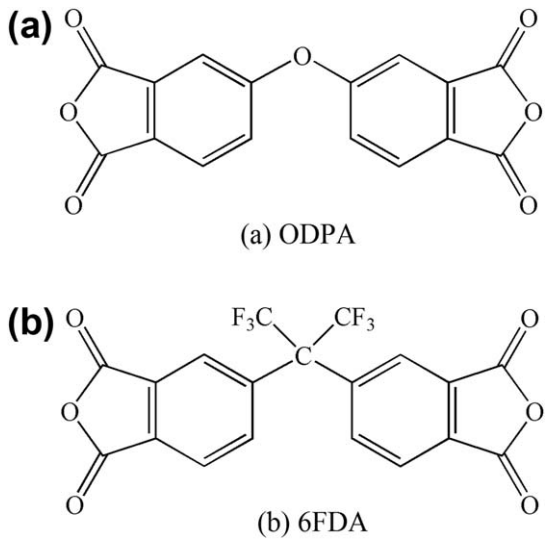

Figure 1. Chemical structure of (a) ODPA, (b) 6FDA.

interactions between CNTs and PI chains containing aromatic rings.[6] Naotoshi et al.[7] showed that totally aromatic PIs are highly capable of solubilizing a large amount of single-walled CNTs. Moreover, great efforts have been made to investigate interfacial interactions between aromatic polymers and CNTs to reinforce composites. Kar et al.[15] showed that aromatic groups directly interact with nanotubes by π–π stacking. Zaiser[16] show that the interactions between aromatic polymes and CNT were strongly influenced by the specific monomer structure. Avila-Orta et al.[17] showed that carbon nanotubes could serve as templates for the nucleation of semicrystalline polymers containg aromatic rings through π–π interaction due to their aromatic structure. Although these studies have provided some insights into the nature of nanoscale dispersion of nanotubes in PI matrix and their interfacial interactions at nanoscale meter, the efficient reinforcement mechanism on the optimum nanoscale dispersion and interfacial bonding between nanotubes and polymer chains still requires deep elucidation.

With a significant improvement of mechanical properties as our main objective, we have selected two benzoxazole-containing PIs as the matrix for CNTs. The two PIs are synthesized from the reactions of using the same diamine with different dianhydrides. The chemical structure of the two dianhydrides was shown in Figure 1. Both PIs exhibit similar chemical structure, only differ in ether linkage or bulky CF_3 groups between two benzene rings in dianhydrides. This allow us to compare mechanical behavior of the two nanocomposite series and assign differences in mechanical behavior directly to the PI structure or the interfacial architecture for the preferred conformation and packing arrangement of aromatic PI molecules on nanotubes. The influences of carboxylation of CNTs on the nanoscopic dispersion state of nanotubes in PI matrix were investigated, thereon modified nanotubes were chosen as reinforcement for two PI-based nanocomposites. Strain–stress behavior and SEM of fracture surface were measured to reveal that good interfacial interaction is required to achieve stress transfer across the nanotube–matrix interface, a necessary condition for improving the mechanical properties of polymer composites. Furthermore, a model for the preferred conformation adopted by a single linear and nonlinear PI chain on a single CNT were established to elucidate the nature of interactions between PI chains and nanotubes at the molecular level.

EXPERIMENTAL

Materials

5-Amino-2-(*p*-aminophenyl) benzoxazole (AAPB, 99.71%, obtained from Harbin Institute of Technology), 4.4-hexafluoroisopropyl di-phthalic anhydride (6FDA, Fluorochem) and 4,4′-oxydiphthalic anhydride (ODPA, purity 99.7%, Shanghai Research Institute of Synthetic Resins) were used as received. *N*, *N*-Dimethylacetamide (DMAc) was distilled before use. The pristine multiwalled CNTs and multiwalled COOH-CNTs (purity 99.9%) synthesized by catalytic chemical vapor deposition (CVD) with outer diameter of 30–50 nm, inner diameter 5–12 nm and length of 10–20 μm were supplied by Chengdu Organic Chemicals, Chinese Academy of Science.

Preparation of Neat PI and CNT/PI Nanocomposites

The PI (AAPB/ODPA and AAPB/6FDA) were synthesized by the traditional two-step method. The poly (amid acid) (PAA) was synthesized by the polycondensation of AAPB and ODPA or AAPB and 6FDA dissolved in DMAc. The PAA was thermally imidized to form PI. The CNT/PI nanocomposites were prepared by in-situ polymerization. The polymerization of CNT/PI (AAPB/ODPA) nanocomposites was illustrated in Figure 2. The details were summarized below. First, the COOH-CNTs were dispersed in the solution with AAPB dissolved in DMAc in an ultrasonic bath at 47 kHz for 3 h to obtain a AAPB/CNT suspension solution. This stage is very important because the —COOH groups on the CNT surfaces were allowed to react with the amine groups ($—NH_2$) of AAPB, which rendered the COOH-CNTs dispersible in the AAPB solution. Next, ODPA was added to the COOH-CNTs /AAPB suspension solution. After the reaction mixture was stirred at 300 rpm at room temperature 6 h, a stable high viscous CNT/PAA solution was obtained. The entire reaction was carried out by stirring in a nitrogen purged three-neck round bottom flask immersed in an ultrasonic bath. Finally, the resulting CNT/PAA solution was cast on to clean glass plates and dried in a dry air-flowing chamber at 90°C for 10 h. Then, the films, 40–60 μm, were cured stepwise in vacuum at 350°C to obtain the solvent-free films and subsequently cool to room temperature. The other PI (AAPB/6FDA)-based nanocomposites were also synthesized in the same procedure. To compare the dispersibility of nanotubes in solution, both pristine CNTs and COOH-CNTs s with same 0.5 wt % loading were added to the solution with AAPB dissolved in DMAc to obtain suspension solution in an ultrasonic bath at 47 kHz for 3 h. The nanoscale dispersion of nanotubes in the suspension solutions was monitored by TEM.

Characterization

The FT-IR spectra of pristine CNTs, COOH-CNTs, AAPB, COOH-CNT/AAPB, PIs, and CNT/PI nanocomposites were recorded at room temperature in the range of 400–4000 cm^{-1} by Bruker Vector 22 system. The Raman spectra of carbon nanotubes, PIs and CNT/PI nanocomposites were obtained with

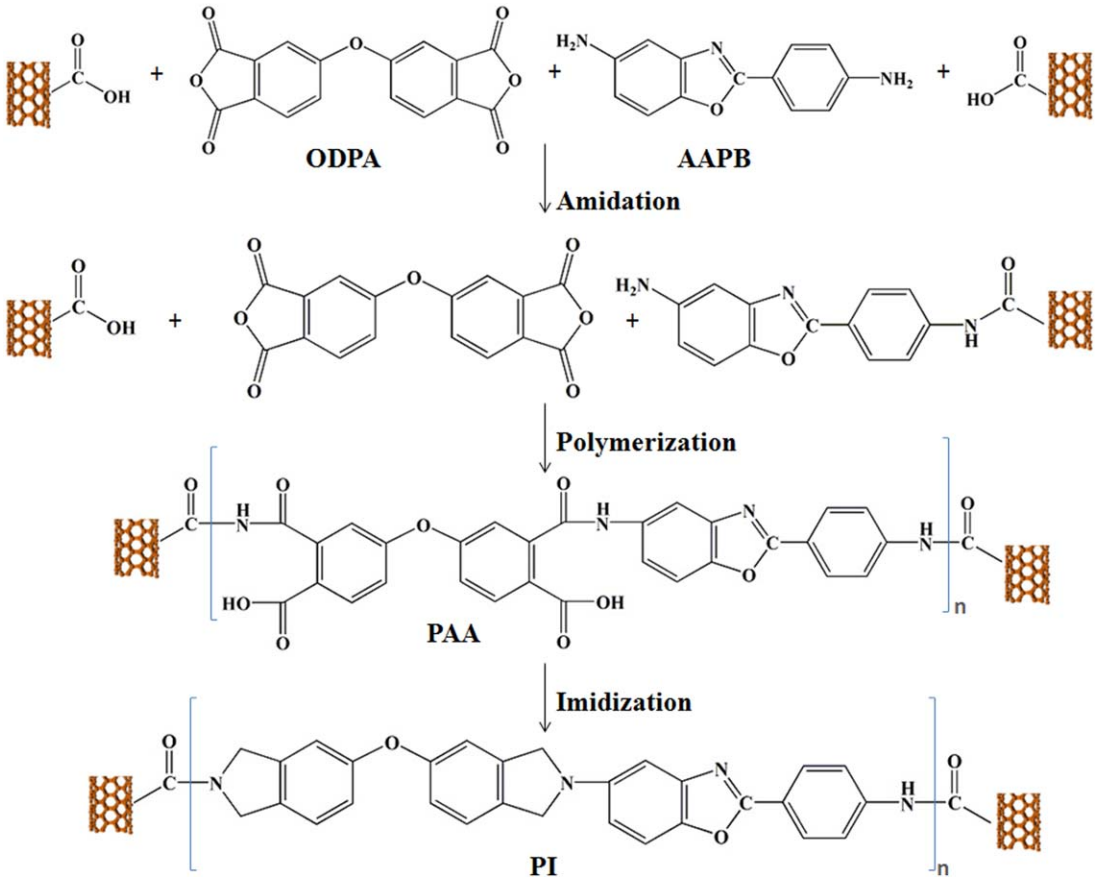

Figure 2. Schematic illustration for *in situ* polymerization of CNT/PI(AAPB/ODPA) nanocomposites in the presence of COOH-CNTs. [Color figure can be viewed in the online issue, which is available at wileyonlinelibrary.com.]

a JOBIN Yvon Horiba Raman Spectrometer Model HR800 with 632.8 nm line from a helium/neon laser. The TEM images were obtained using Hitachi H-7650 field emission transmission electron microscope (Japan) at an acceleration voltage of 100 kV. The Quanta 200F SEM was used to characterize the morphology of the fracture surfaces of CNT/PI nanocomposite films. To decrease the charge effect under the SEM analysis, the samples were sputter-coated with a thin layer (ca. 3 nm) of Au prior to SEM imaging. The tensile tests of the films with the dimensions of 2 × 30 mm^2 were carried out in the uniaxial extension mode using universal mechanical test system UTS-10 (Germany) at room temperature according to ASTM D638.

RESULTS AND DISCUSSION

Nanotube Dispersion and Its Interaction with PIs

The FT-IR spectra of pristine CNTs and COOH-CNTs were presented in Figure 3. The peak at 1630 cm^{-1} is ascribed to stretching vibrations of C═C bond forming the framework of carbon nanotubes sidewalls. The peak at 1400 cm^{-1} correspond to deformation vibrations of C—H. The peaks at 1094, 1045 cm^{-1} assigned to a mixture of stretching and deformation vibrations of C—O were observed. Compared with the spectrum of pristine CNTs, new peaks at 1740 and 3440 cm^{-1} were ascribed to stretching vibrations of C═O bond and stretching vibrations of O—H bond of carboxylic acid groups of COOH-CNTs, respectively. Thus, FT-IR spectra confirm that nanotubes were well modified with carboxylic acid groups.

To compare the dispersion quality of pristine CNTs and COOH-CNTs, the CNT—AAPB/DMAc solution was cast on a round 400 mesh copper grids to make free standing film and visualized by TEM, as shown in Figure 4. Long individual

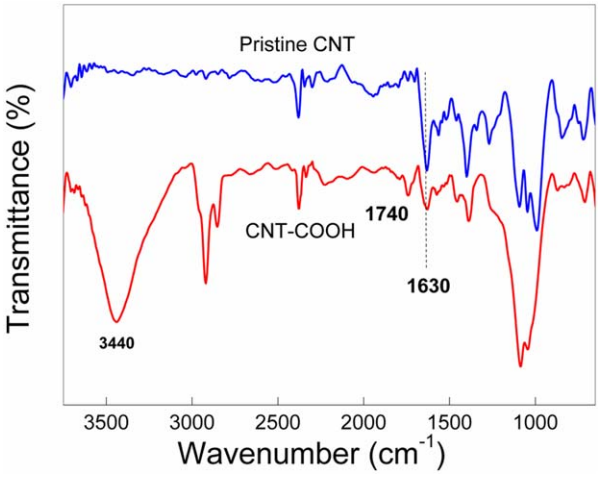

Figure 3. FT-IR spectra of pristine CNTs and COOH-CNTs. [Color figure can be viewed in the online issue, which is available at wileyonlinelibrary.com.]

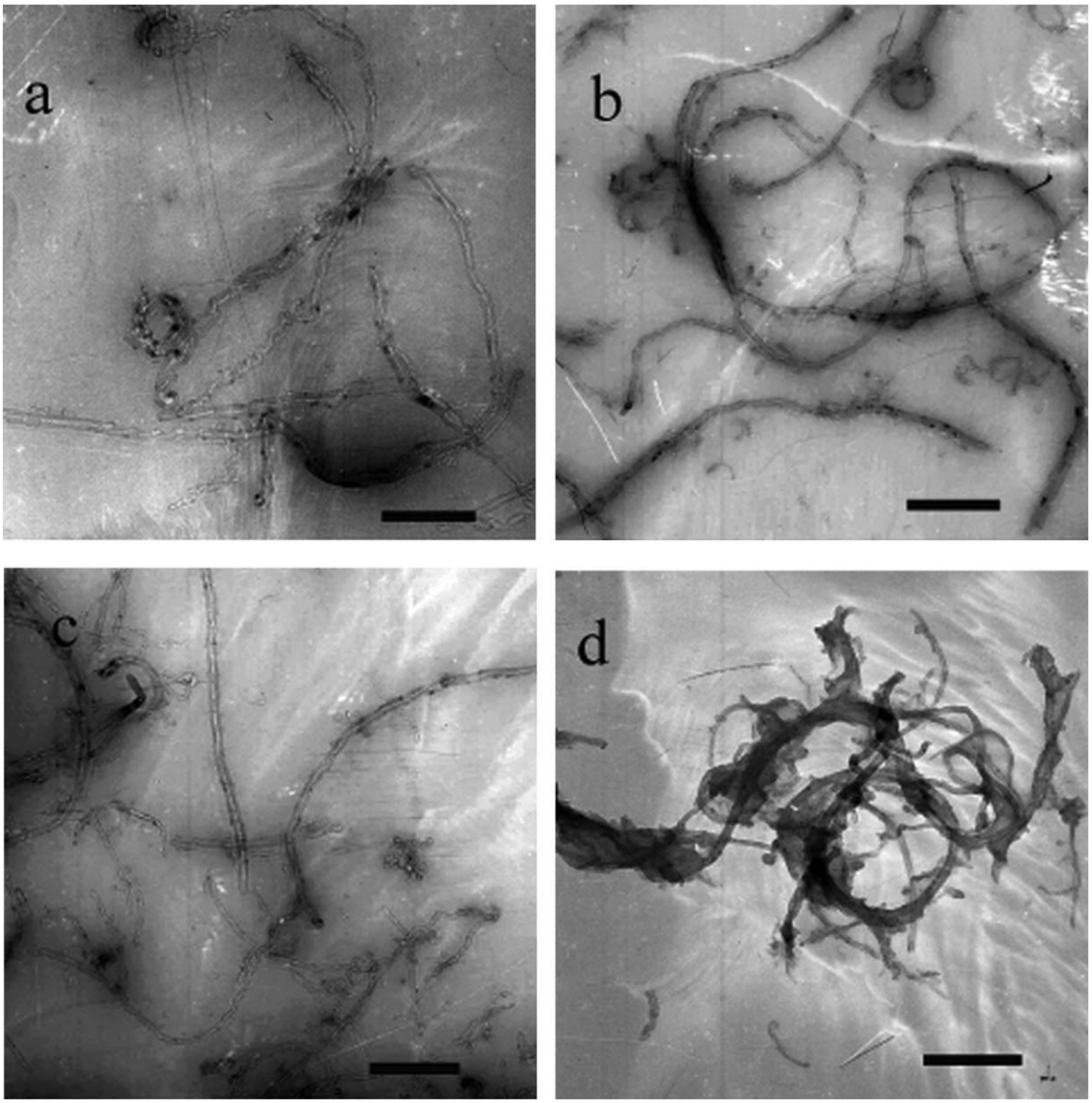

Figure 4. TEM micrographs of CNTs in solution of AAPB/DMAc with (a) 0.25 wt % COOH-CNTs, (b) 0.5 wt % COOH-CNTs, (c) 0.75 wt % COOH-CNTs, (d) 0.5 wt % pristine CNT (scale bar: 200 nm).

nanotubes were dispersed homogeneously in COOH-CNTs/AAPB solution with 0.25 and 0.5 wt % CNT. The entire lengths of nanotubes could not be observed in the micrographs [Figure 4(a,b)] because they were longer than the scales of the figures. In contrast, the nanotubes in pristine CNT/AAPB solution with 0.5 wt % CNT kept their original assemblies, tangled with each other [Figure 3(d)]. The results indicated that the potential amidation between the amine groups of AAPB and —COOHs groups of the COOH-CNTs disentangled nanotubes agglomerates and improved the miscibility of CNTs with diamine through chemical bonding. However, when the COOH-CNTs s concentration was increased to 0.75 wt %, the dispersion state was not as uniform as that in COOH-CNTs/AAPB solutions with COOH-CNTs loadings of 0.25 and 0.5 wt %. Further isolated CNT-rich regions appear. These results indicated that nanotubes tend to aggregate due to the sufficient interactions between nanotubes at high concentration [Figure 4(c)].

To investigate the mixing-induced amidation of the —COOH groups on the CNT surface with the amine groups (—NH_2) of AAPB, the FT-IR spectrum of solvent-free COOH-CNTs/AAPB powders was compared to that of AAPB. Their spectra were given in Figure 5. The peak at 1643 cm^{-1} was assigned to C═N of benzoxazole ring in the AAPB spectrum, whereas the peak at 1646 cm^{-1} was attributed to C═O stretching vibration in amide group (Amid I) in COOH-CNTs/AAPB spectrum that overlap with the peak assigned to C═N in the benzoxazole ring. Two peaks at 1556 and 1570 cm^{-1} (a combination of N—H deformation vibration and C—N stretching vibration in Amid II) were observed in COOH-CNTs/AAPB spectrum. The changes in characteristic peaks prove the formation of

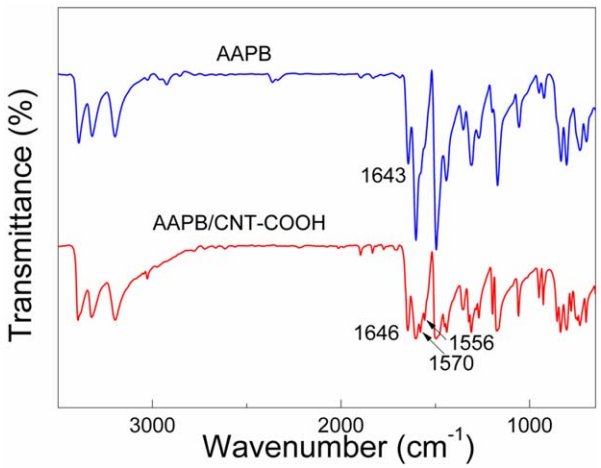

Figure 5. FT-IR spectra of AAPB and COOH-CNTs/AAPB. [Color figure can be viewed in the online issue, which is available at wileyonlinelibrary.com.]

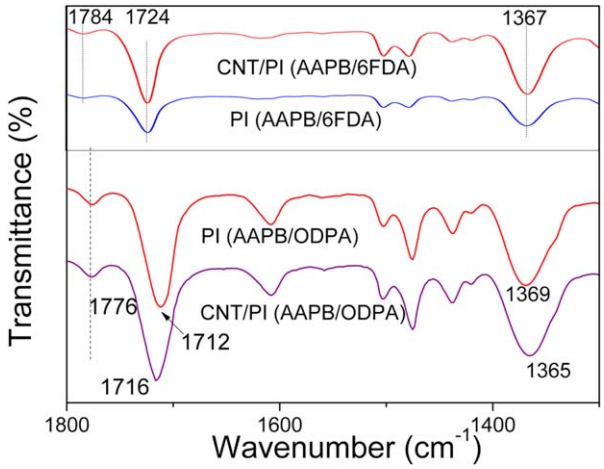

Figure 6. FT-IR spectra of PI (AAPB/6FDA), PI (AAPB/ODPA) and their nanocomposites with CNTs. [Color figure can be viewed in the online issue, which is available at wileyonlinelibrary.com.]

C(═O)NH linkage in the COOH-CNTs/AAPB and confirm that the amidation occurred between AAPB and COOH-CNTs.

The diamine plays a double role for the *in situ* polymerization, a dispersant to disentangle the CNT agglomerates and a monomer for PI synthesis with dianhydrides. The highly aromatic PAA can favorably interact with the graphene surface of the nanotubes via π–π overlap interaction, which prevent nanotubes from tangling with each other and thereby stabilizing the solution.[6] Furthermore, due to the carboxylic acid group in each unit of the PAA backbone, the COOH-CNTs were assumed to interact with PAA by hydrogen bonding to further stabilize the solution.[18,19] Thus, both PAAs, although differ in chemical structure and conformation, form the same interaction with the nanotubes. This results in homogeneous dispersion of individual nanotubes in both PI matrices.[20]

The FT-IR spectroscopy was further used to study the interfacial interactions between nanotubes and two PI chains, and the results were presented in Figure 6. The nonlinear PI (AAPB/6FDA) demonstrate characteristic peaks at 1724, 1784, and 1367 cm^{-1} which were assigned to the asymmetric and the symmetric stretching of C═O bonds and inplane stretching of C—N bonds in the imide ring, respectively.[21] After nanotubes are incorporated into the PI (AAPB/6FDA), there was no shift in the above characteristic peaks. On the contrary, after incorporating nanotubes, the linear PI (AAPB/ODPA) nanocomposites show an opposite trend compared to nonlinear PI (AAPB/6FDA). Obvious shift in the characteristic peaks were observed. The peak originally at 1369 cm^{-1}, assigned to stretching of C—N bonds in imide ring shift to 1365 cm^{-1}; and the peak originally at 1712 cm^{-1}, ascribed to the symmetric of C═O bonds in the imide ring, shift to 1716 cm^{-1}. The results indicated that the PI (AAPB/ODPA) might interact with nanotubes via π–π interaction,[22] while the π–π interaction between PI (AAPB/6FDA) and nanotubes was impeded due to the space steric effect induced by the bulky CF_3 side groups in the PI (AAPB/6FDA). Therefore, the interfacial interaction between CNT and PI (AAPB/ODPA) is stronger than that between CNT and PI (AAPB/6FDA).

The π–π interaction between CNT and PI (AAPB/ODPA) backbone was verified by Raman spectra. Figure 77 shows Raman spectra of COOH-CNT, PI, and CNT/PI (AAPB/ODPA) nanocomposite. A band at approximately 1323 cm^{-1} in the Raman spectrum of COOH-CNTs was assigned to the D-band, which originated from the sp^2 hybridized disorder in the graphitic structure. Another G-band at 1568 cm^{-1} was attributed to the inplane vibrations of the graphitic wall.[23] This band was used to investigate the load transfer from PI matrix to CNTs in nanocomposites for the presence of polymer coating substantially affects the vibration of tangential movement of the graphitic wall, indicating the strong force between polymer backbone and graphene sheet.[24] Comparing G-band of CNT/PI (AAPB-ODPA) nanocomposites to that of COOH-CNTs, an upshift of 8 cm^{-1} from 1568 to 1575 cm^{-1} was observed. This upshift indicated that the electronic environment of the nanotubes surface was changed, which was attributed to π–π interactions between aromatic rings of PI(AAPB-ODPA) backbone and

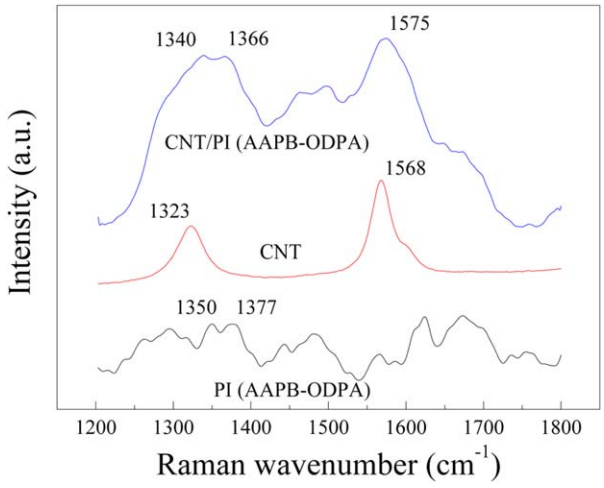

Figure 7. Raman spectra of CNTs, PI (AAPB-ODPA) and CNT/PI (AAPB-ODPA) nanocomposites with 0.5 wt % COOH-CNTs. [Color figure can be viewed in the online issue, which is available at wileyonlinelibrary.com.]

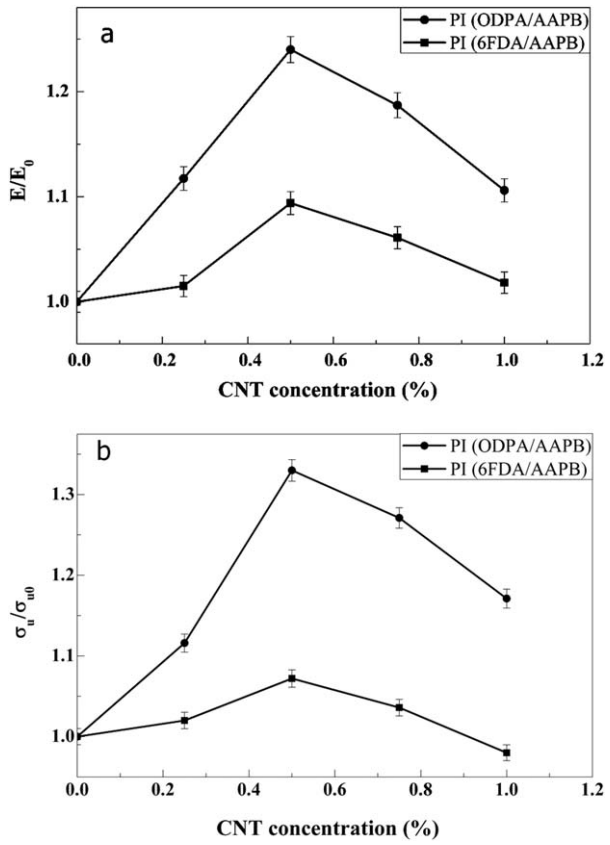

Figure 8. Impacts of CNTs on mechanical properties of CNT/PI nanocomposites. (a) Young's modulus and (b) break stress.

the underlying graphene sheet on the sidewall of nanotubes.[25] In addition, when the spectra of PI(AAPB-ODPA) and CNT/PI(AAPB-ODPA) nanocomposites were compared, it was found that the bands at 1350 and 1377 cm^{-1} ascribed to C—N and C—C stretching of the aromatic rings in PI(AAPB-ODPA) downshift to 1340 and 1366 cm^{-1} in the CNT/PI(AAPB-ODPA) nanocomposite spectrum, respectively.[21,26–28] These shifts indicated that the vibrational structure of the PI(AAPB-ODPA) was altered due to the binding on to CNT graphene sheet, which suggests the significant alteration of PI(AAPB-ODPA) chain conformation due to π–π interaction with nanotubes.

Stress–Strain Behavior of Nanocomposites

The relationship between the concentration of nanotubes and Young's modulus and break stress of the nanocomposites was shown in Figure 8(a,b), respectively. The Young's modulus (E_0) and break stress (σ_{u0}) of the neat PI (AAPB-6FDA) were found to be 3.30 GPa and 138 MPa, respectively; whereas those of PI (AAPB-ODPA) were 3.75 GPa and 181 MPa, respectively. Compared with neat PIs, an addition of 0.25 wt % CNTs results in the increment of Young's modulus (E) and break stress (σ_u). An addition of 0.5 wt % CNTs results in higher Young's modulus and break stress than that of 0.25 wt % CNTs. However, the Young's modulus and break stress decrease due to stress concentration induced by aggregation at CNTs loadings of 0.75 wt %. For both CNT/PI nanocomposites, the modulus and break stress increase with the nanotubes concentration at low loadings and the best enhancement was obtained at CNTs loading of 0.5 wt %. The results indicated that there is a critical CNT concentration between 0.5 and 0.75 wt %, below which the strengthening effect for CNT/PI nanocomposites increases with increase of CNT concentration. Above this critical CNT concentration, however, the modulus and break stress of CNT/PI nanocomposites decrease. In particular, the break stress even decrease below that of the neat PI matrix at CNTs loadings of 1 wt % due to aggregation effect of nanotubes at a high concentration. These mechanical results are in agreement with the previous TEM characterization on the nanoscale dispersion, indicating that homogeneous dispersion of individual nanotubes in surrounding matrix would be a major factor in enhancing the modulus and strength of nanocomposites. Introducing CNTs into PI

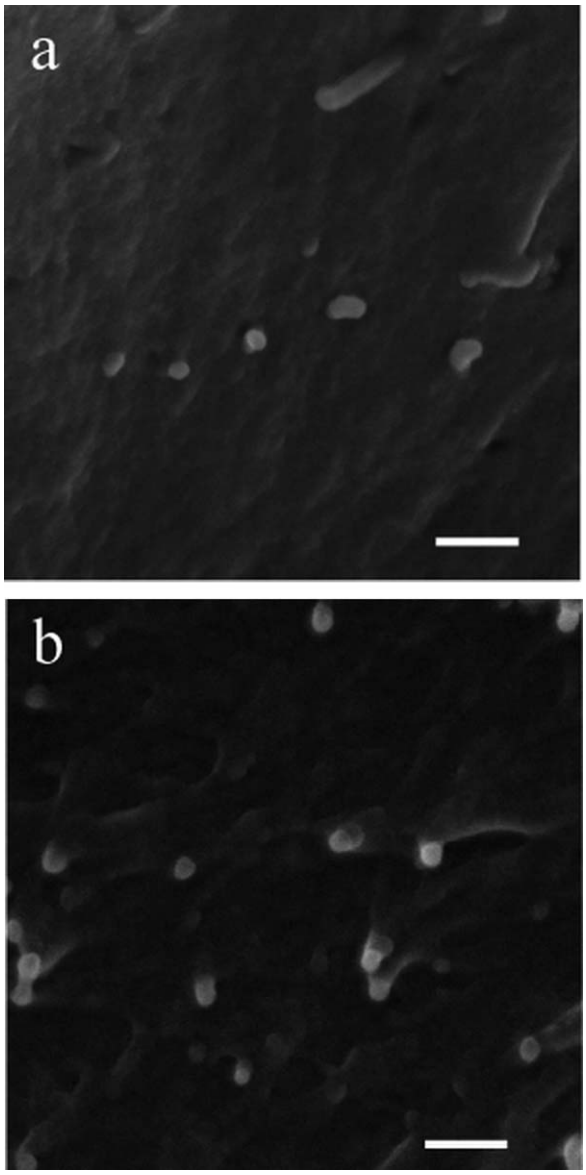

Figure 9. SEM images of the edges resulted from stretching both PIs containing 0.5 wt % COOH-CNTs to failure. (a) PI (AAPB/6FDA), (b) PI (AAPB/ODPA) (scale bar 200 nm).

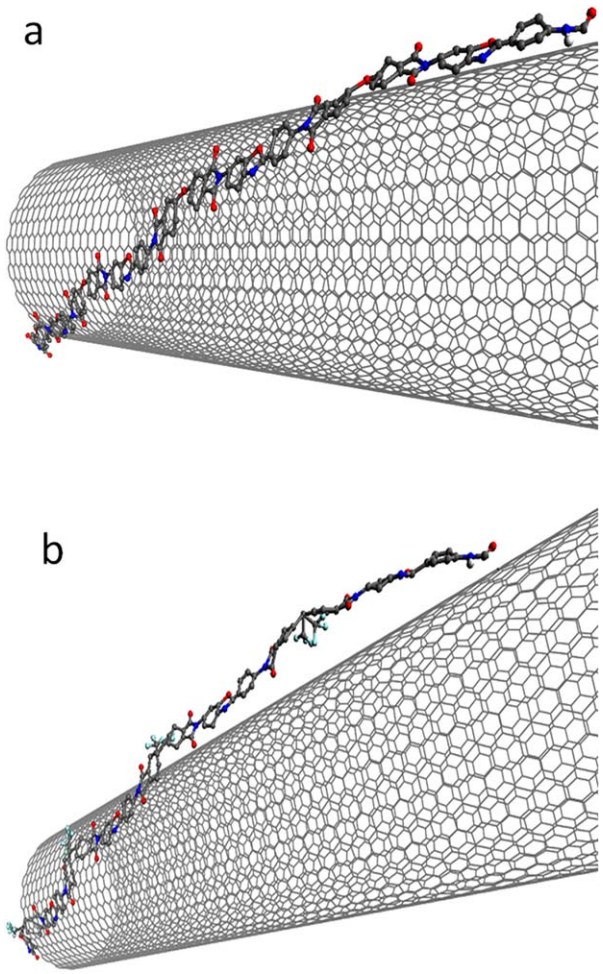

Figure 10. Scheme of preferred conformation adopted by a single PI chain on a single CNT. (a) PI (AAPB/ODPA), (b) PI (AAPB/6FDA). [Color figure can be viewed in the online issue, which is available at wileyonlinelibrary.com.]

(AAPB-6FDA) matrix has a slight influence on the Young's modulus and break stress. The maximum increases in Young's modulus and break stress are 9 and 7%, respectively. In contrast, significant changes arise in PI(AAPB-ODPA) matrix, and the maximum increase in Young's modulus and break stress are 24 and 33%, respectively. This fact reflect a more pronounced reinforcement effect for the PI (AAPB-ODPA) matrix than PI (AAPB-6FDA) matrix.

To further study the nature of the difference in reinforcement, the fracture surface of nanocomposites after tensile test was monitored by SEM, as shown in Figure 9. Individual nanotubes were uniformly dispersed in both nanocomposites, indicating a good dispersion because of modification of nanotubes surface. It was clearly seen that the nanotubes appeared poor-wetted by the nonlinear PI matrix. Furthermore, the SEM image of fracture surface display traces of holes which were left after pulling out of nanotubes from the PI (AAPB-6FDA) matrix, which is considered as evidence for weak stress transfer from nonlinear PI matrix to nanotubes during deformation [Figure 9(a)]. In contrast, protruded nanotubes appeared well-wetted by the linear PI coating, as shown in Figure 9(b). The CNT/PI (AAPB-ODPA) nanocomposites did not break at the polymer–nanotube interfaces, suggesting that the polymer in the vicinity of nanotubes be stronger than bulk polymer as well as high level of interaction between the nanotubes and the surrounding polymer. This offers sufficient stress transfer from nanotubes to PI matrix. The results indicated that the conformation of PI chains had strong influences on the polymer architecture on the surface of nanotubes, consequently affecting the interfacial interactions between nanotubes and PI chains.

In general, the hexagonal arrangement in the graphene sheet of CNTs is isomorphic to the wrapping atomic arrangement of carbon atoms in the aromatic rings on the PI backbone. Therefore aromatic rings tend to interact with nanotubes strongly via π–π interactions and form an ordered assembly of PI strands on the surface of nanotubes. However, the PI strands on the underlying hexagonal graphene sheet is determined not only by local π–π interactions, but also by the overall PI chain geometry and flexibility.[29] Since the mentioned PIs have similar highly aromatic chemical structure, differing only in conformation, the preferred conformation of PI chain on CNT is reflected in the energetically favorable conformation adopt by PI chains at the interface that maximizes the π–π interactions. A proposed model for the preferred conformation adopted by a single PI chain on a single CNT is presented, which was shown in Figure 10. Both PI chains have the same aromatic benzoxazole group, which tends to increase the PI rigidity and improve interchain packing regularity. The flexible ether linkage within the linear PI (AAPB-ODPA) chain allows the PI backbone a certain degree of flexibility, which in turn allows the PI backbone to adopt an energetically favorable conformation with its aromatic rings interacting with the hexagonal graphene lattice of the substrate CNTs [Figure 10(a)]. Thus an ordering interfacial architecture with high strength formed between PI (AAPB-ODPA) chains and nanotubes. In contrast, the introduction of steric bulky CF_3 side group in nonlinear PI (AAPB-6FDA) make the main chain rigid and hard to rotate, which hinder the intimate contact with nanotubes, and consequently inhibit favorable π–π interactions and prevent those chains from adopting low energy conformations that readily interact with the nanotubes surface [Figure 10(a)]. Comparing the nonlinear PI (AAPB-6FDA) with the bulky CF_3 groups, linear PI (AAPB-ODPA) can adopt an energetically favorable conformation that maximize the π–π interactions between aromatic rings of PI backbone and the underlying graphene sheet at the surface of nanotubes.

CONCLUSIONS

A stable dispersion of disentangled CNTs was obtained by combining covalent with noncovalent functionalization of nanobubes synergistically. The greatest enhancement was achieved at CNT/PI(AAPB-ODPA) nanocomposites with COOH–CNT loading of 0.5 wt %. This results revealed that the nanoscale dispersion of disentangled nanotubes in the aromatic PI matrix and interfacial architecture of an ordered assembly of PI strands on the surface of nanotubes via π–π interactions play an important roles in determining the mechanical properties of resulting nanocomposites. This study also suggested that the geometry and flexibility of aromatic PI be critical in determining the

preferred conformation of PI chains on the surface of CNTs, which controls the interfacial architecture and interfacial interactions. Future research on the nature of π–π interactions between aromatic rings of PI(AAPB-ODPA) backbone and the underlying graphene sheet at the surface of nanotubes is currently in process.

ACKNOWLEDGMENTS

The financial support from National Natural Science Foundation of China (No. 51010005, 91216123, 51174063), the program for New Century Excellent Talents in University (NCET-08–0168), Natural Science Funds for Distinguished Young Scholar of Heilongjiang Province, and the Project of International Cooperation supported by Ministry of Science and Technology of China (2013DFR10630) are acknowledged. The authors would like to thank Dr. Yulia G. Bogdanova from Chemistry Department of Moscow Lomonosov State University and Dr. Julia V. Kostina from A.V.Topchiev Institute of Petrochemical Synthesis of the Russian Academy of Sciences for valuable discussion on FT-IR.

REFERENCES

1. Zuo, H. J.; Chen, J. S.; Yang, H. X.; Hu, A. J.; Fan, L.; Yang, S. Y. *J. Appl. Polym. Sci.* **2008**, *107*, 755.
2. Ghosh, M. K.; Mittal, K. L. *Polyim. Fundam. Appl.* **1996**, *36*, 2.
3. Pérez, R. *J. Appl. Polym. Sci.* **2009**, *113*, 2264.
4. Iijima, S. *Nature* **1991**, *354*, 56.
5. Andrews, R.; Weisenberger M. *Curr. Opin. Solid State Mater. Sci.* **2004**, *8*, 31.
6. Park, C.; Ounaies, Z.; Watson, A. *Chem. Phys. Lett.* **2002**, *364*, 303.
7. Shigeta, M.; Komatsu, M.; Nakashima, N. *Chem. Phys. Lett.* **2006**, *418*, 115.
8. Yudin, V. E.; Svetlichnyi, V. M.; Shumakov, A. N.; Letenko, G. D., Feldman, Y. A., Marom, G. *Macromol. Rapid. Commun.* **2005**, *26*, 885.
9. Wall, A.; Coleman, J. N.; Ferreira, M. *Phys. Rev. B* **2005**, *71*, 125421.
10. Steuerman, D. W.; Star, A.; Narizzano, R. *J. Phys. Chem. B* **2002**, *106*, 3124.
11. Bahr, J. L.; Mickelson, E. T.; Bronikowski, M. *J. Chem. Commun.* **2012**, *12*, 193.
12. Hirsch, A. *Angew. Chem. Int. Ed.* **2002**, *41*, 1853.
13. Holzinger, M.; Vostrowsky, O.; Hirsch, A. S. *Angew. Chem. Int. Ed.* **2001**, *40*, 4002.
14. Ghosh, A.; Rao, K. V.; Voggu, R.; George, J. S. *Chem. Phys. Lett.* **2010**, *488*, 198.
15. Kar, T.; Bettinger, H. F.; Scheiner, S. *J. Phys. Chem. C* **2008**, *112*, 20070.
16. Yang, M.; Koutsos, V.; Zaiser, M. *J. Phys. Chem. B* **2005**, *109*, 10009.
17. Espinoza-Martínez, A.; Avila-Orta, C.; Cruz-Delgado, V. *J. Nanomater.* **2012**, *2012*, 189820.
18. Srivastava, R.; Banerjee, S.; Jehnichen, D. *Macromol. Mater. Eng.* **2009**, *294*, 96.
19. Chen, J.; Liu, H.; Weimer, W. A. *J. Am. Chem. Soc.* **2002**, *124*, 9034.
20. Dror, Y.; Pyckhout-Hintzen, W.; Cohen, Y. *Macromolecules* **2005**, *38*, 7828.
21. Ishida, H.; Wellinghoff, S. T.; Baer, E. *Macromolecules* **1980**, *13*, 826.
22. Kuila, B. K.; Malik, S.; Batabyal, S. K. *Macromolecules* **2007**, *40*, 278.
23. Kukovecz, A.; Kramberger, C.; Georgakilas, V. *Eur. Phys. J. B Cond. Matter Complex Syst.* **2002**, *28*, 223.
24. Sinani, V. A.; Gheith, M. K.; Yaroslavov, A. A. *J. Am. Chem. Soc.* **2005**, *127*, 3463.
25. Yuan, W.; Feng, J.; Judeh, Z. *Chem. Mater.* **2010**, *22*, 6542.
26. Schwan, J.; Ulrich, S.; Batori, V. *J. Appl. Phys.* **1996**, *80*, 440.
27. Gu, X. *Appl. Phys. Lett.* **1993**, *62*, 1568.
28. Mottaghitalab, V.; Xi, B.; Spinks G. M. *Synth. Met.* **2006**, *156*, 796.
29. Gurevitch, I.; Srebnik, S. J. *Chem. Phys.* **2008**, *12*, 144901.